Thin Solid Films 535 (2013) 296–301

Contents lists available at SciVerse ScienceDirect

Thin Solid Films

journal homepage: www.elsevier.com/locate/tsf

Advanced electrical simulation of thin film solar cells

Marc Burgelman *, Koen Decock, Samira Khelifi, Aimi Abass

University of Gent, Electronics and Information Systems (ELIS), Pietersnieuwstraat 41, B-9000 Gent, Belgium

ARTICLE INFO

Available online 25 October 2012

Keywords:
Solar cell
Numerical modelling
SCAPS
Metastable defects

ABSTRACT

Advanced electrical simulation of copper indium gallium diselenide solar cells is illustrated by setting up a demonstration case in SCAPS (Solar Cell Capacitance Simulator), the solar cell simulation programme of the University of Gent. The model includes band gap grading, multivalent defects and metastable transitions between defects. This simplified demonstration model clearly and quantitatively illustrates some topics that were extensively discussed in recent literature: metastable defects exist in either an acceptor or in a donor configuration; the occupation of these configurations is set during initial conditions at higher temperature, and then frozen in during cell operation at lower temperature. These occupations can strongly influence the effective doping profile in the absorber, and hence possible energy barriers in the structure. The dependence of such barriers on the initial conditions and on the operating voltage can cause a considerable dependence of the current–voltage characteristics on the initial conditions, especially of the fill factor. At the same time, the demonstration model illustrates some of the recent extensions of SCAPS.

1. Introduction

Electrical and optical numerical simulations of thin film solar cells are becoming a common practice [1]. The state-of-the art polycrystalline thin film solar cells, copper indium gallium diselenide (CIGS) and cadmium telluride (CdTe), and the advanced structures under study are however ever more complicated. Also, our actual insights in the materials properties of the chalcogenides unveil complicated phenomena and mechanisms, a notorious example being the metastable states of various kinds in CIGS materials, for an overview see e.g. [2]. Software tools for numerical simulation of solar cells need to keep pace with these evolutions.

The electrical solar cell simulation programme SCAPS (Solar Cell Capacitance Simulator) is a development of the University of Gent, and is available to the photovoltaic research community [3]. In the past few years until very recently, its capabilities have been enhanced as will be illustrated in this paper: (i) Grading of band gap and all other semiconductor properties [4]; this has become a key feature in modern CIGS cell structures [5]. (ii) Defects with multiple occupation states [6]; amphoteric states not only in amorphous Si are well known, but also several important defects in CIGS are multivalent. (iii) Our knowledge on defects that can change their configuration state (donor or acceptor) in a metastable way is by now quite well established [7–11]; SCAPS can now simulate the effects of these sophisticated materials properties to measured cell characteristics [12]. (iv) Several tunnel mechanisms and defect interlayers are essential to describe bifacial cells and tandem and multi-junction cells.

The aim of this article is to illustrate some of the recent extensions of SCAPS to perform advanced electrical simulation. We will set up and study a model for a solar cell with copper indium gallium sulphoselenide absorber $(Cu(In,Ga)(Se,S)_2$ or CIGS) and illustrate the simulated effects of band gap grading and of multivalent and metastable defects. The purpose is to demonstrate that SCAPS can handle such complicated material properties, and to illustrate how these properties influence the metastable cell behaviour. It is not the purpose to set up a model for some specific cell and to calibrate the model against measurements.

2. Advanced material properties in solar cell modelling

2.1. Graded material properties

The advantages of alloying pure $CuInSe_2$ with either gallium or sulphur were recognised early. Not only absorbers with a somewhat wider, and thus closer to optimum band gap could be realised in the same materials system, but also band gap engineering became possible where one strives for an optimum profile $E_g(x)$ of the band gap by controlling the materials composition y and z of the $Cu(In_{1-y}Ga_y)(Se_{1-z}S_z)_2$ absorber as a function of the depth x in the cell. The numerical treatment of band gap 'grading' was developed more than a decade ago, e.g. [13,14]. As the band gap is a material property that is a function of the material composition, thus $E_g(y,z)$ in the example of double graded CIGSSe above, a grading of the materials composition $y(x)$ and also $z(x)$ in the case of double grading, also causes a grading of other material properties, e.g. electron affinity $\chi(y)$, effective density of states $N_C(y)$ and $N_V(y)$, mobility $\mu_n(y)$ and $\mu_p(y)$, dielectric constant $\varepsilon(y)$, and optical absorption $\alpha(\lambda,y)$… The presence of graded properties results in extra driving terms in the semiconductor equations,

* Corresponding author. Tel.: +32 9 264 3381; fax: +32 9 264 3594.
E-mail address: Marc.Burgelman@elis.ugent.be (M. Burgelman).

0040-6090/$ – see front matter © 2012 Elsevier B.V. All rights reserved.
http://dx.doi.org/10.1016/j.tsf.2012.10.032

proportional to their gradients ∇E_g and $\nabla\chi$…; see e.g. [15]. The approach followed in SCAPS is materials oriented [4]: one has to provide a grading profile of the composition $y(x)$, and the composition dependence of all graded parameters $E_g(y)$…; both can be specified in a user file or set by a variety of internal models. The programme then calculates all $E_g[y(x)]$ dependencies. Some properties cannot be considered as material properties, but are also determined by technology, impurities… and can also be graded, e.g. by diffusion. Therefore, SCAPS allows that the grading profile of the shallow doping densities $N_D(x)$ and $N_A(x)$ and of defect densities $N_t(x)$ are defined directly and not via the composition.

2.2. Multivalent defects

Multivalent defects have more than two charge states, and are hence characterised by more than one energy level; this is in contrast with single donors (charge states 0 and +1) and acceptors (charge states 0 and −1). Obvious examples of a multivalent state are amphoteric states in amorphous silicon that have charge states of −1, 0 and +1. Simulation programmes intended for a-Si solar cells, e.g. ASA, had amphoteric states implemented right from the beginning [16]. However, some defects in CIGS are also multivalent: double acceptors (charge states −2/−1/0) were reported: Na_{III} and O_{Se} [17] and Cu_{III} [18], and even triple acceptors (−3/−2/−1/0), e.g. an indium or gallium vacancy V_{III} [18]. SCAPS now implements the tri-state defects amphoteric, double acceptor and double donor, and user defined defects with up to five charge states and thus four energy levels [6]. In most cases, tri-state defects can be adequately described by introducing two single level defects, but this is not always the case [19]. Also, the correct description of multivalent defects is essential in the treatment of metastable transitions between defects (see next section).

2.3. Metastable defects

The result of measurements performed on CIGS based solar cells depends on the history of the sample; this has been ascribed to the properties of metastable defect states present in CIGS semiconductors [20]. An overview of the effects observed and of the actual insights in metastable defects in CIGS can be found in [10,11]. Most of our knowledge on the properties of these metastable states and of the transitions between them is based on first principles calculations by Lany, Zunger and co-workers [7–9,18].

Two type of metastable defects were described, one based on a selenium vacancy (V_{Se}) and one based on a substitutional group III defect on a Cu site (In_{Cu} or Ga_{Cu}). As copper vacancies (V_{Cu}) are abundant in most CIGS materials (e.g. [2]), and as these V_{Cu} vacancies readily form complexes with other native defects, the metastable defects in CIGS are most prominent in their complexed form: (V_{Se}–V_{Cu}) or 'double vacancy defect', and (In_{Cu}–$2V_{Cu}$) or its gallium equivalent (Ga_{Cu}–$2V_{Cu}$). Both defects are either in an acceptor or in a donor configuration, where they behave as a normal (sometimes multivalent) defect. The (reversible) transitions between both configuration states are governed by rate equations that are thermally activated. It is important to note that the total number of metastable defects is constant during these transition processes; this is in contrast to the situation in amorphous Si based materials, where metastable states can be induced by illumination.

In the demonstration example below, we will only input double vacancy defects, and thus we will limit the further description of metastable defects to this type. In the acceptor configuration, the (V_{Se}–V_{Cu}) defect behaves as a 4-state acceptor; however, the level associated with the −2/−3 transition lies in the conduction band, hence a description as a double acceptor is adequate. The 0/−1 transition level is close to the valence band, and the −1/−2 transition level close to, but below the conduction band edge. In the donor configuration, the (V_{Se}–V_{Cu}) defect behaves as a single donor with a 0/+1 transition level close to the conduction band (Fig. 1).

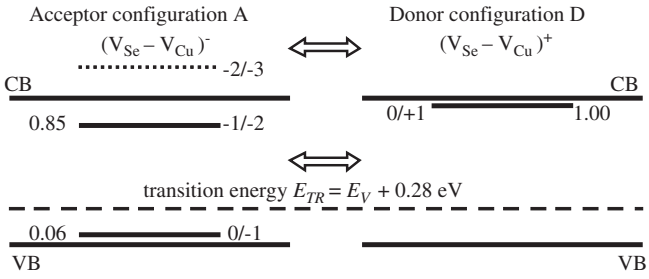

Fig. 1. Schematic overview of the defect levels and metastable transition associated with the (V_{Se}–V_{Cu}) complex in $CuInSe_2$ (E_g = 1.04 eV). The energy levels as used in the model of Table 1 are in eV and referred to the top of the valence band.

The transition between the two configurations involves a double capture/emission process; e.g. the D→A transition in Fig. 1 involves an electron capture followed by a hole emission; and the A→D transition involves the capture of two holes. As a result of these transitions, in equilibrium there is a fraction f_A of the metastable states in the acceptor configuration, and a fraction f_D in the donor configuration, with $f_A + f_D = 1$. As the transitions are thermally activated, their rate is much higher at higher temperature. Usually it is observed that metastable transitions proceed under initial or annealing conditions at $T > 300$–330 K, but are inhibited under measuring conditions at $T < 250$ K; these conditions can be set in laboratory experiments. In real solar cell operation conditions, metastable adaptations can thus occur during operation.

Under equilibrium conditions, that is $V = 0$ and dark, a physical interpretation can be given to the transition energy E_{TR} in Fig. 1. When the Fermi level E_F is above E_{TR}, the metastable states are predominantly in the acceptor configuration, thus $f_A \approx 1$ and $f_D \to 0$; when E_F is below E_{TR}, the metastable states are predominantly in the donor configuration, thus $f_D \approx 1$ and $f_A \to 0$; when $E_F = E_{TR}$, then $f_A = f_D = 1/2$. In non-equilibrium, thus when the cell is illuminated or when a voltage is applied, the Fermi level splits up in E_{Fn} and E_{Fp}, and the simple rule of thumb above can no longer be applied. The occupations f_A and f_D then follow from the rate equations as formulated in [8,12]. These rate equations depend on both the local electron and the hole densities, thus the complete band diagram, this is the evolution of the band edges $E_C(x)$ and $E_V(x)$ and of the Fermi levels $E_{Fn}(x)$ and $E_{Fp}(x)$. When the density of metastable states is high, the band diagram depends on the charge contained in them; on the other hand, the charge in the metastable states depends on f_A and f_D, that depend on the band diagram. The occupation of the configuration states f_A and f_D thus should

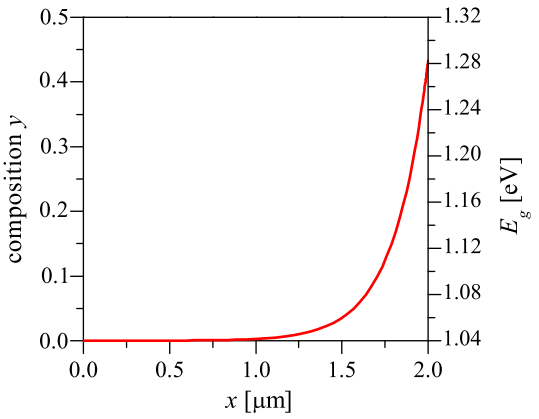

Fig. 2. Profile of the composition profile $y(x)$ of the $CuIn_{1-y}Ga_ySe_2$ absorber assumed in the model. The profile is exponential with $y(0) = 0$ at the back contact, $y(d) = 0.432$ at the buffer, corresponding to $E_g(d) = 1.28$ eV, and with $L_{char,\ right} = 0.2$ μm. The band gap is given on the right y axis.

Table 1
Summary of the input parameters of the SCAPS demonstration model. The contacts are ohmic ('flat-band').

			Absorber	Buffer	Window
			$Cu(In,Ga)Se_2$	CdS	ZnO
Composition (see text)	$y(x)$		Exponential Fig. 2	–	–
Thickness	d	μm	2	0.05	0.2
Band gap (see text)	E_g	eV	1.04–1.68 parabolic, $b=0.15$	2.42	3.3
Electron affinity (see text)	χ	eV	4.30	4.30	4.445
Shallow doping density	N_A, N_D	cm^{-3}	7×10^{15}, A	10^{17}, D	5×10^{17}, D
Recombination defect					
Density	N_t	cm^{-3}	1.4×10^{14}	10^{17}	2×10^{17}
Type			A	Neutral	D
Level	E_t	eV	$E_V+0.33$	$E_V+1.2$	$E_V+1.7$
Metastable states (notation and definition of symbols: see [12])					
Density	N_M	cm^{-3}	10^{16}		
Transition energy	E_{TR}	eV	$E_V+0.280$		
Activation energy	ΔE_{EC}	eV	0.100		
Activation energy	ΔE_{HC}	eV	0.350		
Activation energy	ΔE_{EE}	eV	0.825		
Activation energy	ΔE_{HE}	eV	0.910		
Acceptor conf. level 0/−1		eV	$E_V+0.06$		
Acceptor conf. level −1/−2		eV	$E_V+0.85$		
Donor conf. level 0/+1		eV	$E_V+1.00$		

To set the occupation of the metastable configurations, initial conditions have to be provided, see Table 2; we adopt the common nomenclature from the literature, e.g. [10].

be obtained by an iterative calculation. This was done in [12] and implemented in SCAPS.

3. A demonstration cell model

The presence of metastable states is in itself not sufficient to explain the metastable behaviour of a solar cell, e.g. its current–voltage (I–V) or current density–voltage (J–V), capacitance–voltage (C–V) or capacitance–frequency (C–f) characteristics. It is also necessary that a metastable change in the $f_A(x)$, $f_D(x)$ distributions cause a substantial change in the band diagram, e.g. a change in some barrier, that in turn influences the cell characteristics [10]. Usually it is assumed that such barrier occurs at the buffer–window side of the semiconductor [10,11,21,22] and can be caused (i) by a highly doped surface region of the absorber, caused by the metastable states themselves or by a defected surface layer, (ii) by possibly metastable changes in the buffer layer, (iii) by charged interface states at the absorber/buffer or (iv) buffer/window layer. In all cases it is essential that the model for the absorber–buffer–window range is very accurate,

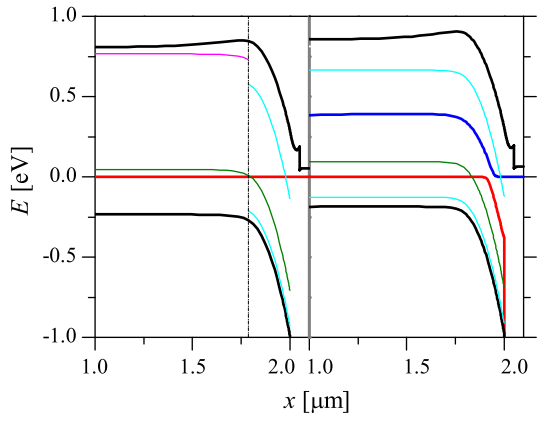

Fig. 3. Band diagrams under the initial conditions of Table 2. Left: relaxed; the black vertical line marks the transition from (predominantly) donor configuration ($x<1.76$ μm) to acceptor configuration ($x>1.76$ μm). Right: light soaked; the absorber is almost completely in the acceptor configuration. The curves shown are black: E_C, E_V; red E_F (left) or E_{Fp} (right); dark blue: E_{Fn} (right); E_{TR}: green; the two levels of the metastable acceptor configuration: light blue; the level of the metastable donor configuration: pink.

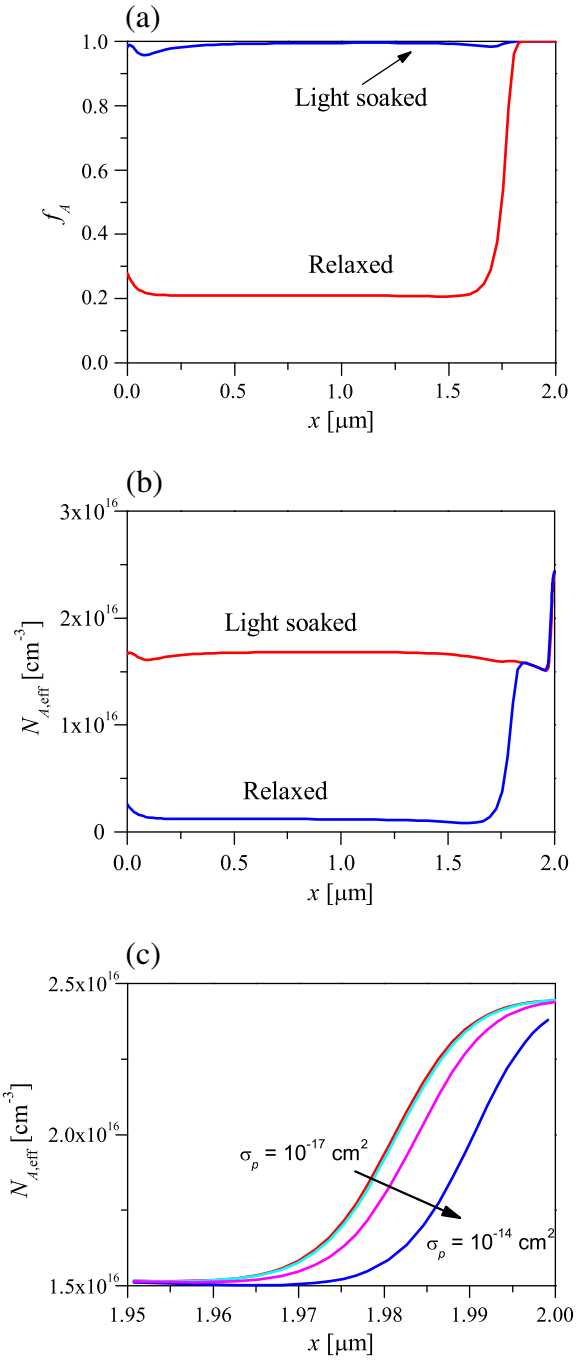

Fig. 4. (a) Occupation f_A of the metastable acceptor configuration and (b) the resulting effective doping density $N_{A,eff}$ (see text). The calculations are the initial conditions relaxed (red) and light soaked (blue) as specified in Table 2. (c) Detail of (b) close to the buffer layer. The capture cross sections of the −1/−2 level of the acceptor configuration are: $\sigma_n=10^{-17}$ cm^{-2} and $\sigma_p=10^{-17}$ (red), 10^{-16} (cyan), 10^{-15} (magenta) and 10^{-14} cm^2.

Table 2
Initial conditions to set the metastable configuration. For all conditions, $T=330$ K. When illumination is present, an AM1.5G spectrum is assumed.

Initial condition	V (Volt)	Intensity (sun)	Pass filter
Relaxed	0	0	
Light soaked	0	1	–
Forward	+0.5	0	
Reverse	−1.0	0	
Red light soak	0	1	$\lambda>700$ nm
Blue light soak	0	1	$\lambda<450$ nm
Red-on-bias	−1.0	1	$\lambda>700$ nm

The equilibrium band diagram in the relaxed state is shown in Fig. 3.

both electronically and optically; this is so because the A↔D transitions are very sensitive to the electron density close to the absorber surface. Setting up such a model is a research by its own, that we consider outside the scope of this article. Here we will assume a simple model and demonstrate how metastable defect transitions can provoke metastable *I–V* behaviour in the cell. Any resemblance to a specific cell or technology is not claimed here. In this model, the barrier is caused by band gap grading in the absorber, and is completely located in the absorber region [23]. Doing so, we demonstrate three of the recent additions to SCAPS: grading, multivalent defects, and metastable defects.

We assume a $CuIn_{1-y}Ga_ySe_2$ absorber layer with exponentially graded composition profile $y(x)$ as shown in Fig. 2. The band gap of the quaternary absorber varies parabolically from 1.04 eV ($y=0$, pure $CuInSe_2$) to 1.68 eV ($y=1$, pure $CuGaSe_2$), with a bowing factor $b=0.15$ eV; the electron affinity is quasi independent of the composition; this situation is called 'E_C grading'. The main input parameters of the model are given in Table 1; the complete SCAPS definition file can be requested from the authors.

4. Discussion

4.1. Metastable configuration and effective doping density

Under equilibrium, the occupation of the metastable configurations f_A and f_D can be estimated from the position of the transition energy E_{TR} (green curve in Fig. 3, left, for relaxed initial conditions) relative to the Fermi level E_F (red line in Fig. 3). For $x>1.75$ μm, $E_F>E_{TR}$ and the acceptor configuration dominates, $f_A\approx1$. Assuming that the metastable acceptor has charge −1, the effective doping density is $N_{A,\mathrm{eff}}=N_A+N_M\approx1.7\times10^{16}$ cm^{-3} (notations and values of Table 1; the charge in the acceptor type defect at $E_V+0.33$ eV is neglected against N_A); very close to the buffer, $x>1.97$ μm, E_F crosses the (−1/−2) level

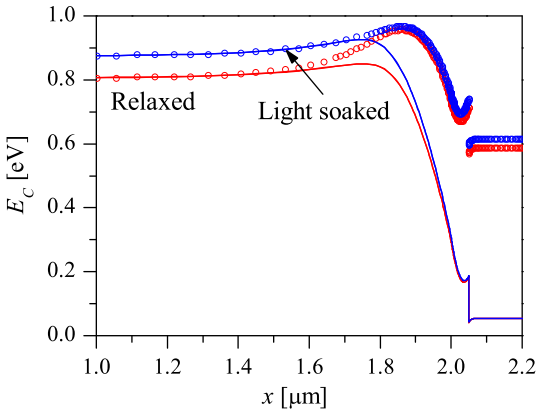

Fig. 5. The barrier in the conduction band, depending on the initial conditions (red: relaxed and blue: light soaked) and on the actual work point (solid line: dark $V=0$ and light at J_{sc} coinciding; open circles: light, at $V=V_{oc}$).

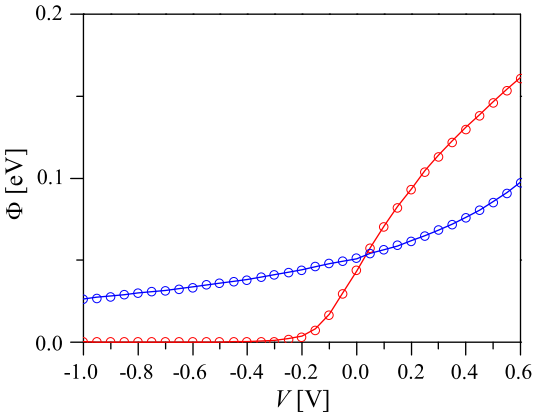

Fig. 6. Energy barriers in the conduction band as a function of applied voltage, in the relaxed (red) or light soaked state (blue). The solid line is calculated in dark, the symbols are calculated under one sun illumination.

of the acceptor configuration (blue in Fig. 3), and we obtain $N_{A,\mathrm{eff}}=N_A+2N_M\approx2.7\times10^{16}$ cm^{-3}. For $x<1.75$, $E_F<E_{TR}$, the metastable donor configuration starts to dominate; however, as $|E_{TR}-E_F|$ is small in the whole CIGS bulk, $f_D\to1$ is not reached, but f_D saturates at $f_D\approx0.8$, thus $f_A\approx0.2$. Then $N_{A,\mathrm{eff}}=N_A+f_AN_M-f_DN_M\approx1\times10^{15}$ cm^{-3}. The metastable occupation $f_A(x)$ and the resulting effective doping density $N_{A,\mathrm{eff}}(x)$ as calculated with SCAPS are shown in Fig. 4.

It is clear from Fig. 4 that in the relaxed state the effective doping density is low in most of the absorber bulk due to compensation of the shallow acceptors by the metastable donors, and that a high effective doping density is obtained close to the junction due to the metastable acceptors: the metastable (V_{Se}–V_{Cu}) state is a natural way to explain a strongly doped surface layer in the absorber, that has often been supposed in the literature. We pointed out that the occupation of the charge states (0/−1/−2) of the acceptor configuration does not depend on the assumed values of the capture cross sections σ_n and σ_p under equilibrium conditions (dark, $V=0$); this is a general property of Shockley–Read–Hall recombination. Under illumination with one sun, only the occupation of the charge state −2 is slightly sensitive to the values of σ_n and σ_p. In our problem, the −1/−2 transition occurs in a 30 nm thin sheet near the buffer layer; this profile shifts with about 10 nm when the σ_n/σ_p ratio is varied between 10^{-3} and 10^{+3} (Fig. 4c).

The situation of the light soaked state (Fig. 3, right) is less clear: the transition energy E_{TR} is in between the two Fermi levels E_{Fn} and E_{Fp}, and the simple rule of thumb does not apply. SCAPS calculations show that the metastable states are in the acceptor configuration, $f_A\approx1$, over the entire absorber; the reason is that the much increased electron density

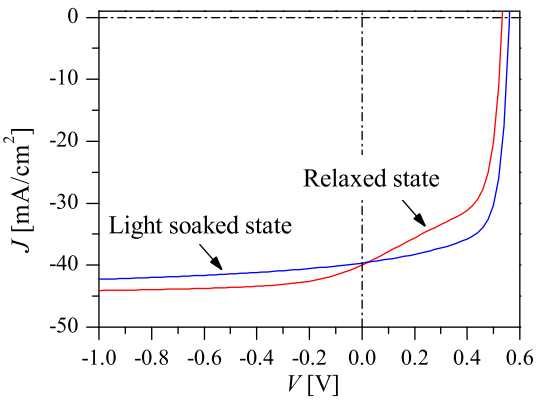

Fig. 7. *J–V* curves calculated at 300 K in the relaxed state (red) and the light soaked state (blue).

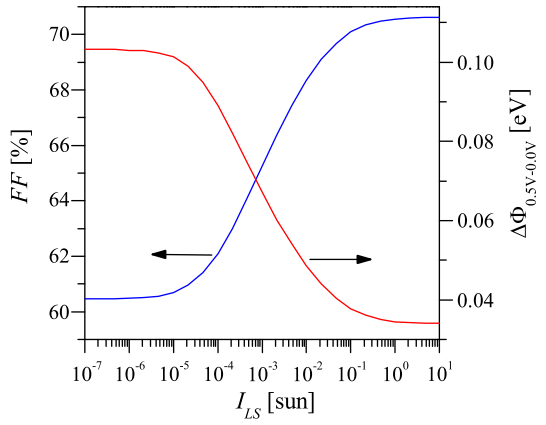

Fig. 8. Calculated fill factor *FF* and difference in barrier height Φ(0.5 V)–Φ(0 V) as a function of the light intensity during light soaking.

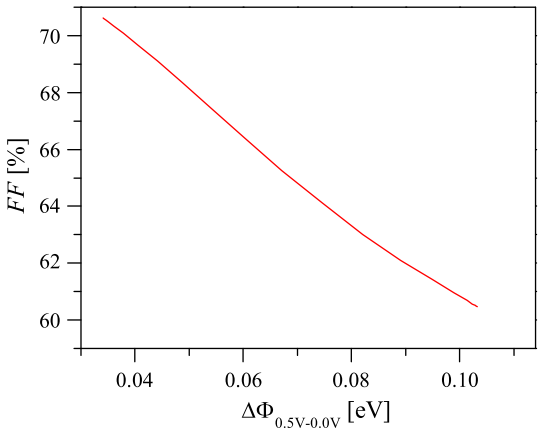

Fig. 10. The relation between barrier height and fill factor.

under light soaking conditions enhances electron capture and hence the D→A transition of Fig. 1. As a result, the effective doping density also is high over the entire absorber (Fig. 4b, blue curve).

4.2. The electron barrier in the absorber

The occupations of the metastable configurations, f_A and f_D, as calculated under one of the initial conditions of Table 2, are frozen in for all subsequent measurement simulations in SCAPS. We will focus here on a feature seen in the band diagrams of Fig. 3: the small hump in the conduction band at $x \approx 1.8$ μm. After having established the initial state (here relaxed or light soaked), the band diagrams were calculated under operation conditions at 300 K and equilibrium, illuminated and at short circuit or open circuit; a detail of the conduction band hump is shown in Fig. 5. It is seen that the hump depends on applied voltage, and is substantially larger at V_{oc} than at $V=0$ (at J_{sc} or equilibrium). Also, the hump at V_{oc} is substantially larger in the relaxed state than in the light soaked state.

A SCAPS script was used to calculate the height of the hump or barrier $\Phi = E_{C,\max} - E_C(0.5\ \mu m)$. The result is shown in Fig. 6. It can be observed that the barrier vanishes at sufficient reverse bias, and almost linearly increases with forward bias voltage, independent of illumination.

4.3. The barrier and the fill factor

It can be conjectured that a barrier in the conduction band impedes the collection of electrons that are generated in the absorber at the left of the barrier. This applies only to electrons generated at $x<1.5$ μm (Fig. 5), this is a rather small fraction of the total generation, due to the strong absorption in CIGS in the 1.5 μm$<x<$2 μm range. Thus the light current reduction is by far not as bad as could be expected from $\exp(-\Phi/kT)$, with $\Phi \approx 50$–100 meV (Fig. 6). However, there will still be some light current reduction, that will be more prominent at forward bias, thus at the maximum power point or at V_{oc} than at zero bias, thus at J_{sc}. Hence we conjecture a fill factor loss associated with the conduction barrier, and especially by its dependence on *V*. A first confirmation is seen in the *I*–*V* curves of Fig. 7, where the fill factor (*FF*) is 10% lower in the relaxed state than in the light soaked state (≈60% vs. ≈70%). The relaxed *J*–*V* curve shows some 'two-diode' behaviour, that has often been observed, and even much more prominent [10].

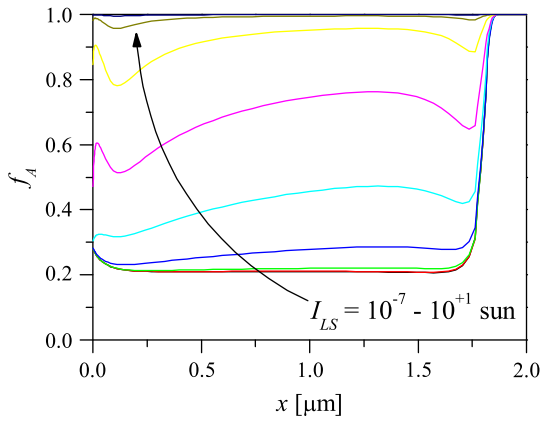

Fig. 9. The occupation f_A of the metastable acceptor configuration, as a function of the light intensity during light soaking.

4.4. Variation of the light soaking conditions

We varied the illumination intensity I_{LS} during light soaking in a wide range from 10^{-7} sun to 10 sun. In Fig. 8 the fill factor *FF* is shown, and in Fig. 9 the occupation f_A of the metastable acceptor state, both as a function of I_{LS}. It can be seen that for $I_{LS}<10^{-4}$ sun, the cell is almost in the relaxed state with low *FF*, and an appreciable occupation of the donor configuration compensates the shallow acceptor doping in most of the absorber ($x<1.75$ μm). For $I_{LS}>0.1$ sun, the cell is almost in the fully light soaked state with high *FF* and a high effective doping density in the entire absorber, due to $f_A \to 1$.

A SCAPS script was used to calculate the difference in barrier height between $V=0.5$ V and $V=0$; this was done as a function of I_{LS} during light soaking, and is also shown in Fig. 8. The resemblance between the two graphs in Fig. 8 suggests a strong (anti-)correlation between the barrier and the fill factor. This is confirmed in Fig. 10: the barrier in the conduction band causes a loss in *FF*.

5. Conclusions

A SCAPS model for a CIGS solar cells was set up that illustrates the capabilities of calculating graded cell structures and multivalent and metastable defect states. In this model, the buffer/window structure was kept simple; in contrast, some sophistication was built into the absorber layer. A band gap grading profile was set that results in a small but influential hump or energy barrier in the conduction band. Metastable states of the double vacancy type (V_{Se}–V_{Cu}) were introduced.

It was shown that the occupation of the metastable configurations (acceptor/donor) strongly depends on the initial conditions, relaxed or light soaked, with strong consequences for the effective doping density in the absorber. These in turn cause the energy barrier in the conduction band to depend both on initial conditions and on voltage during cell operation. By varying the light intensity during light soaking, we could set a practical intensity range for 'dark' during relaxing and 'light' during

light soaking conditions. We also could attribute the fill factor loss in the relaxed state to the stronger voltage dependence of the conduction band barrier. These kinds of simulations were hitherto not possible.

Acknowledgement

We acknowledge the support of the Research Foundation-Flanders (FWO) (K.D., Ph.D. Fellowship).

References

[1] M. Burgelman, J. Verschraegen, S. Degrave, P. Nollet, Prog. Photovoltaics 12 (2–3) (2004) 143.
[2] S. Siebentritt, M. Igalson, C. Persson, S. Lany, Prog. Photovoltaics 18 (6) (2010) 390.
[3] M. Burgelman, P. Nollet, S. Degrave, Thin Solid Films 361 (2000) 527.
[4] M. Burgelman, J. Marlein, in: 23rd European Photovoltaic Solar Energy Conference, WIP, Valencia (E), 2008, p. 2151.
[5] A. Chirilă, S. Buecheler, F. Pianezzi, P. Bloesch, C. Gretener, A.R. Uhl, C. Fella, L. Kranz, J. Perrenoud, S. Seyrling, R. Verma, S. Nishiwaki, Y.E. Romanyuk, G. Bilger, A.N. Tiwari, Nat. Mater. 10 (2011) 857.
[6] K. Decock, S. Khelifi, M. Burgelman, Thin Solid Films 519 (21) (2011) 7481.
[7] S. Lany, A. Zunger, Phys. Rev. B 72 (3) (2005) 035215.
[8] S. Lany, A. Zunger, J. Appl. Phys. 100 (11) (2006) 113725.
[9] S. Lany, A. Zunger, Phys. Rev. Lett. 100 (1) (2008) 016401.
[10] P. Zabierowski, in: A. Bosio, A. Romeo (Eds.), Thin Film Solar Cells: Current Status and Future Trends, Nova Science Publishers, Hauppauge, NY, 2010.
[11] P. Zabierowski, C. Platzer-Björkman, in: 22nd European Photovoltaic Solar Energy Conference, WIP, München, Milan, I, 2007, p. 2395.
[12] K. Decock, P. Zabierowski, M. Burgelman, J. Appl. Phys. 111 (2012) 043703.
[13] O. Lundberg, M. Edoff, L. Stolt, Thin Solid Films 480 (2005) 520.
[14] M. Topič, F. Smole, J. Furlan, J. Appl. Phys. 79 (11) (1996) 8537.
[15] C. Snowden, Introduction to Semiconductor Modelling, World Scientific, 1986.
[16] R.E.I. Schropp, M. Zeman, Amorphous and Microcrystalline Silicon Solar Cells, Kluwer Academic, Norwell, 1998.
[17] S.H. Wei, S.B. Zhang, A. Zunger, J. Appl. Phys. 85 (1999) 7214.
[18] S.H. Wei, S.B. Zhang, A. Zunger, Appl. Phys. Lett. 72 (24) (1998) 3199.
[19] K. Decock, S. Khelifi, M. Burgelman, J. Appl. Phys. 108 (2010) 063707.
[20] M. Igalson, H.W. Schock, J. Appl. Phys. 80 (10) (1996) 5765.
[21] M. Igalson, M. Bodegård, L. Stolt, Sol. Energy Mater. Sol. Cells 80 (2) (2003) 195.
[22] J. Pettersson, M. Edoff, C. Platzer-Björkman, J. Appl. Phys. 111 (1) (2012) 014509.
[23] K. Decock, S. Khelifi, M. Burgelman, in: 25th European Photovoltaic Solar Energy Conference, WIP Valencia (E), 2010, p. 3323.